Postprint of: Wójcik N. A., Wolff S., Karczewski J., Ryl J., Ali S., Effect of crystallinity on structural, thermal, and in vitro dissolution properties of Na_2O-CaO-Nb_2O_5/MgO-P_2O_5 glass-ceramics, Journal of the European Ceramic Society, Vol. 43, Iss. 5 (2023), pp. 2234-2244, DOI: 10.1016/j.jeurceramsoc.2022.12.053.

Effect of crystallinity on structural, thermal, and *in vitro* dissolution properties of Na_2O-CaO-Nb_2O_5/MgO-P_2O_5 glass-ceramics

Natalia Anna Wójcik[1*], Stefania Wolff[1], Jakub Karczewski[1], Jacek Ryl[1], Sharafat Ali[2]

[1]*Advanced Materials Center, Institute of Nanotechnology and Materials Engineering, Gdańsk University of Technology, 11/12 G. Narutowicza Street, 80-233 Gdańsk, Poland*
[2]*Department of Built Environment and Energy Technology, Linnaeus University, 35195 Växjö, Sweden*
**corresponding author:* natalia.wojcik@pg.edu.pl
Keywords: Na-Ca-Nb-P-O glass-ceramics; XPS, FTIR; Thermal properties; *In vitro* dissolution

Abstract

The impact of the crystallinity on structural, thermal, and *in vitro* dissolution properties were examined for Na_2O-CaO-Nb_2O_5/MgO-P_2O_5 glasses/glass-ceramics. Glass-ceramics were synthesized via a spontaneous crystallization process. The Nb content in the materials increased with melting temperature, furthermore, the crystallinity is proportional to the Nb content. The presence of crystalline niobates and phosphates is confirmed by FTIR analysis which is consistent with XRD. The FTIR results indicate that the phosphate network is built of different proportions of Q^2, Q^1, and Q^0 units, depending on the amount and type of crystalline phase. Most of the samples show an improvement in thermal stability. The *in vitro* dissolution test showed that the highest mass loss for most of the samples occurred during the first 6 days of immersion in the PBS solution. The presence of small phosphate crystals favors the deposition of hydroxyapatite on samples' surfaces while the larger niobate crystals dissolve more readily.

1. Introduction

Sodium-calcium-phosphate glasses are well-known as non-toxic, biodegradable, and highly biocompatible with the human body [1-3]. They exhibit fast dissolution properties, favorable for bioactive materials [4]. Upon exposure to body fluids, an amorphous calcium phosphate

layer forms that subsequently crystallize into bio-mimetic hydroxyapatite ([HAP, $Ca_{10}(PO_4)_6(OH)_2$]) that provides a strong bone-glass interface [5, 6]. However, too high dissolution rate in body fluids may be a limitation for the practical application of phosphate glasses. Degradation rates can be varied from hours to several weeks by changing the glass composition [7, 8]. The CaO content decreased the dissolution rate of phosphate glasses in distilled water and simulated body fluid (SBF) due to the enhancement of the phosphate network. Furthermore, the cytotoxicity of the Na-Ca-P-O glass system also decreased with an increase in the CaO and a decrease in the P_2O_5 content [9-12]. Niobium addition can significantly improve the thermal stability and chemical durability of phosphate glasses and glass-ceramics [13-16]. In addition, niobium has been shown to stimulate mineralization in human osteoblast populations [17].

Previously, we have reported that phosphate glasses can dissolve high content of niobate from the Nb-crucible during high-temperature melting [14, 15, 18]. This is because phosphates exhibit a high solubility for niobates and that large amounts of niobates can be introduced into phosphate glasses without causing any tendency toward crystallization [16]. On the other hand, bioactive glass-ceramics are also of great interest as crystallinity can help to control the dissolution process. It has been shown that precipitation of the crystal phases: calcium phosphates and niobium oxide in the calcium pyrophosphate glass-ceramics improved the chemical durability and their ability to form apatite in SBF [19, 20]. Glass-ceramic can be prepared in different ways, in the current work, we prepared glass-ceramics by spontaneous crystallization. Nowadays, the spontaneous crystallization of glasses that can occur during fast cooling is of great interest as a new technique of glass-ceramic preparation [15, 21, 22]. Spontaneous crystallization is hard to control and can occur in materials with a high tendency to undergo liquid immiscibility. Consequently, one of the liquid phases is richer in phase which easily forms the crystalline phase. We have shown previously, that spontaneous crystallization

can proceed in phosphate glasses re-melting with Mg metal and nitride under a nitrogen atmosphere at high temperature [15]. The aim of this work is to apprehend the influence of Mg metal and nitrides e.g., Ca_3N_2/Mg_3N_2 as well as niobium dissolution on the phosphate glasses' spontaneous crystallization and to determine the possibility of controlling it.

In this paper, the preparation of Nb-rich bioactive phosphate glass-ceramics, is described. The crystallization process was done through high-temperature re-melting of target glass with Mg and Ca_3N_2/Mg_3N_2. The target Na-Ca-P-O glass compositions doped with Nb or Nb and Mg in similar total contents (10 mol%) were chosen as the most promising and interesting ones based on our earlier findings [13]. The first chosen composition contains 5 mol% of Nb_2O_5 and 5 mol% of MgO while the second 10 mol% only of Nb_2O_5. Both compositions were found to be with the lowest amount of Al as it may slow down the *in vitro* dissolution for higher contents. The choices were also dictated by the study of the effect of reaction/mixing/dissolution of added sources of magnesium/niobium crucible with magnesium and niobium contained in the composition. The structure, thermal, and *in vitro* dissolution properties were studied and analyzed accordingly to find different crystallinity degrees in samples. The presented new biomaterials may be competitive with those actually in use.

2. **Materials and methods**

2.1.Glass preparation

Two series of glass-ceramics were prepared by using the two-step technique. In the first series xNb the starting composition was: x (Mg – Mg_3N_2/Ca_3N_2) - (100 – x)(15.3Na_2O – 36.2P_2O_5 – 39.3CaO – 7.4Nb_2O_5 – 1.7Al_2O_3) while in the second series xNbyMg the starting composition was: x (Mg – Mg_3N_2) - (100 – x)(14.5Na_2O-37.4P_2O_5-39.9CaO-3Nb_2O_5-3.4MgO-1.7Al_2O_3) in (%mol). The target glasses were synthesized using the traditional melt quenching technique from reagents: Na_2HPO_4 (Acros 99%), NH_6PO_4 (Chempur pure p.a.), $CaCO_3$ (Sigma-Aldrich >99.95%), Nb_2O_5 (Alfa Aesar 99.5 %) and MgO (Chempur p.a.). Melting was

conducted in Al_2O_3 crucibles at a temperature of 1100 ºC, in an air atmosphere. A detailed description of the melting process is described elsewhere [13]. In the second step, 1g of pre-prepared glass was mixed with the appropriate amount of Mg powder and Mg_3N_2 (Alfa Aesar 99.6 %) or Ca_3N_2 (Alfa Aesar 99 %). Next, the mixture was placed in an Nb crucible and heated in a nitrogen atmosphere, using a radio frequency furnace, at a temperature of 1350-1600 ºC, depending on the composition (listed in Tab. 1). The melting time was about 1 h. The melts were cooled by switching off the furnace at the end of the run. It took approximately 1 hour for melt to cool to room temperature, and the mean cooling rate for samples was between 21 and 26 ºC min^{-1}. Samples 9Nb and 4Nb3Mg were re-melted due to the high reaction of Mg with nitrogen.

2.2.Morphology and structure characterization

The morphology of the re-melted samples were examined by using scanning electron microscope (SEM), FEI Company Quanta FEG250 in backscatter electron imaging mode at 10 kV acceleration voltage. The compositions were measured on fractured samples using energy dispersive X-ray spectrometer (EDX GENESIS Apex Apollo X60 Spectrometer) and the measurements were conducted on at least 3 different areas for each sample. The structure of the samples were examined by X-ray photoelectron spectroscopy (XPS) and X-ray powder diffraction (XRPD). The high-resolution XPS analyses were performed using an Escalab 250Xi device (ThermoFisher Scientific, USA), equipped with a monochromatic AlKα source. The adventitious carbon C 1s peak at 284.6 eV was used for the X-axis calibration of the XPS spectra. The XRD spectra was recorded on powdered samples at room temperature. The measurement was carried out on a Bruker D2 PHASER diffractometer with CuKα radiation (l = 1.5406 Å) and LynxEye-XE detector with a 2θ range of 5 º to 70º. The data collection lasted for 1 h per sample. The possible errors of XRD results were minimalized by removing the background and are included in the thickness of curves lines.

The structure was also studied using IR spectroscopy. Powdered samples were mixed with KBr powder and pressed using a hydraulic press to obtain plane-parallel plates. Measurements were performed using FTIR spectrometer (PerkinElmer). The IR spectra were scanned 64 times for each sample in the range of 400 – 4000 cm^{-1} with a resolution of 4 cm^{-1}. The IR spectra were also background-corrected only in the range of 400 – 800 cm^{-1} and normalized to the dominating band at ~1100 cm^{-1}. The bands positions were estimated using the Origin software and with precise ± 2 cm^{-1}.

2.3.Thermal properties

The thermal properties of prepared samples were checked using differential scanning calorimetry (DSC). The measurements were done for about 20 mg of powdered samples placed in the Al_2O_3 crucibles in nitrogen atmosphere using Netzsch STA 449 F1 instrument. The maximum temperature of the tests was 1000 °C with heating rate of 20 °C min^{-1}. The glass transition temperature (T_g) was estimated based on the onset of an endothermic drift on the DSC signal while the exothermic maxima found in all samples are assigned to crystallization processes (T_{cr}). The results were analyzed using Proteus software provided by NETZSCH which gives the precision of ± 2 % for the estimations of the parameters.

2.4.In vitro dissolution in PBS

The *in vitro* dissolution process was studied in phosphate-buffered saline solution (PBS) under dynamic conditions. The PBS (Fisher BioReagents) solution (0.01 M phosphate buffer, 0.0027 M potassium chloride and 0.137 M sodium chloride) was prepared by dissolving the tablet in 200 ml deionized water. The PBS has a pH of 7.4 at a temperature of 20 ^oC before starting the tests. Analysis was carried out by adding 20 ml of PBS to 80 mg of powdered samples. The solid samples were ground up into powders in a mortar. The mean size of obtained powder granules was 2.0 ± 0.2 μm estimated for 40 different granules for each sample by microscopic observations. The tests were conducted using an incubating orbital shaker Labnet

314NbS (at ambient atmosphere) with a rotation speed of 120 rpm and temperature of 36.6 °C. The dynamic conditions were simulated by changing the PBS solution every other day. The *in vitro* measurements were performed parallel for two weighted powders of each sample for each endpoint, i.e., 6 and 13 days. After immersion, the samples were rinsed in deionized water and dried in a desiccator for 24 hours.

The total percentage change in weight was calculated based on the mass before and after the immersion in PBS. The topography of samples was observed by using an Olympus LEXT OLS4000 Confocal Scanning Laser Microscope (CSLM). Color imaging was conducted under white LED light and 3D images were obtained using a 405 nm laser and photomultiplier detector. The maximum used objective lens and laser 3D image magnification was 100x, with an optical magnification of 2160x. The structure of the samples immersed in PBS for 6 and 13 days, was examined with XRD and FTIR. The pH of the PBS solution was measured every second day before solution exchange. In addition, 3 consecutive pH measurement points were applied to check the differences between every consecutive measurement. The mean value of all obtained results for each composition was taken as the representative one. Calibration of the pH meter (Elmetron CPC-411) was carried out using three different pH standards (pH 4, 7 and 9).

3. Results and discussion

3.1. The topography and structure

Two series of glassy samples with different compositions and crystallinity were synthesized through re-melting the target glasses: 0Nb, and 0NbMg with Mg metal and Mg_3N_2/Ca_3N_2. The obtained compositions and summary of the melting process are listed in Tab. 1. The samples are labeled according to the Nb content in the glass and in series NbMg the Mg content is also taken into account.

Table 1. Samples IDs, EDX composition, doping x, synthesis temperature (ST) and melting time (MT) for all samples.

Glass code	Na	Ca	Mg	Nb	P	Al	O	Doping x (%mol)	ST (°C)	MT (min)
Series Nb										
x ($Mg – Mg_3N_2/Ca_3N_2$) - (100 – x)($15.3Na_2O – 36.2P_2O_5 – 39.3CaO – 7.4Nb_2O_5 – 1.7Al_2O_3$) in (%mol)										
0Nb	7	9	0	3.4	16.5	0.8	63.4	0	1100	30
3Nb	7.1	11.4	0.25	3.4	15.1	0.5	62.3	$1Mg-2Ca_3N_2$	1350	60
4Nb	11.0	9.2	0	4.5	13.6	0.7	61.0	$1Ca_3N_2$	1400	60
5Nb	9.0	9.6	0.9	5.4	12.8	0.7	61.6	$1Mg-1Mg_3N_2$	1400	60
6Nb	8.7	10.9	0.2	5.8	12.3	0.5	61.5	$1Mg-1\ Ca_3N_2$	1400	60
7Nb	11.9	8.5	2.7	6.5	10.0	0.7	59.6	$1Mg-2Mg_3N_2$	1550	60
9Nb*	10.5	11.5	1.5	9.4	7.1	0.2	59.8	$1Mg-3Mg_3N_2$	1600 1500	10 60
Series NbMg										
x ($Mg – Mg_3N_2$) - (100 – x)($14.5Na_2O$-$37.4P_2O_5$-39.9CaO-$3Nb_2O_5$-3.4MgO-$1.7Al_2O_3$) in (%mol)										
0NbMg	6.9	9.3	0.8	1.4	17.7	0.8	62.9	0		
2Nb4Mg	9.1	11.2	3.57	2.5	13.2	0.8	59.7	$1Mg-3Mg_3N_2$	1400	60
3Nb2Mg	9.4	9.3	2.3	2.9	14.6	0.6	60.9	$2Mg-1Mg_3N_2$	1400	60
3Nb1Mg	7.2	12.7	1.7	3.1	13.5	0.9	60.9	$1Mg-1Mg_3N_2$	1400	60
4Nb3Mg*	9.9	9.2	3.1	4.3	12.5	0.7	60.3	$1Mg-2Mg_3N_2$	1300 1450	10 45
12Nb2Mg	6.9	11.0	1.9	11.8	6.2	0.4	61.8	$3Mg-1Mg_3N_2$	1500	60

*re-melted sample.

In series Nb a clear correlation between the increase of the Nb content and consequently the decrease of the P content is perceptible, no nitrogen was detected by doping the pristine glass with the magnesium or calcium nitride. The lack of nitrogen incorporation in the glass network can be explained by the high reactivity of nitrides. Both calcium and magnesium

nitrides react with water or even moisture in the air to produce ammonia gas and calcium/magnesium hydroxide [23]. The reaction is rapid and occurred while mixing the ingredients before melting. Moreover, the phosphate glasses exhibit high solubility with niobium and readily react with niobium crucible during melting [14, 15, 18]. The niobium dissolution process is assisted with the increase in melting temperature as observed in both series. In the Nb series, it was observed that increasing the magnesium nitride content leads to an increase in the melting temperature, and consequently, the phosphorus reacts more readily with the niobium crucible and dissolves it. A similar correlation was not found when calcium nitride was doped in the pristine glass. This indicates that the effect of magnesium nitride or hydroxide on melt reactivity is higher than for calcium compounds. To know the incorporation of niobium as metal or oxide form and the possible oxidation and reduction of Mg in the glasses samples, the XPS analysis was conducted on all samples and the results are listed in Tab. 2. The results show that the samples containing more than 0.2 at% of Mg, the Mg was found only in the metallic form [24]. However, niobium is mostly present in oxide Nb_2O_5 form [25] and no Nb metal was detected. The XPS analysis done for niobium is displayed in fig. 1, for sample 12Nb2Mg. It suggested that in series NbMg, the reduction of MgO oxide form to Mg metal occurred during melting as a consequence of adding Mg metal and the dissolution of Nb metal from the crucible material. The synthesis was performed under a nitrogen atmosphere, the total content of oxygen during the melting reaction was too low to allow oxidation of both Mg and Nb. The oxidation process of Nb is the dominating one in this case. The data fitting also revealed the presence of a small amount of niobium Nb^{5+} connected to PO_x units [26]. The total content of Nb increases in samples is consistent with the EDX analysis. Most of the phosphorous occurrence in samples as the units $(PO_4)^{3-}$ or $(P_2O_7)^{4-}$ which suggests a highly disrupted glass network [27-29]. In addition, there is small content of phosphorous such as P_2O_5 oxide [29, 30]. Similarly, calcium and sodium were mostly found to build chemical states: $Ca_3(PO_4)_2$ [31] and

Na_3PO_4 [32], and only small amounts were observed in oxide forms [33, 34]. A trace amount of calcium was also detected in the nitrate form [35], which suggests the possibility of a trace amount of N in the glass network.

Table 2. XPS results of all samples.

IDs	[a]$P2p_3$	[b]$P2p_3$	[c]Na1s	[d]Na1s	[e]$Nb3d_5$	[f]$Nb3d_5$	[g]$Ca2p_3$	[h]$Ca2p_3$	[i]$Ca2p_3$	[j]Mg1s
[k] (eV)	133	135.1	1071	1072.9	207.1	208.6	347.4	346.6	348.9	1303.8
Series xNb										
3Nb	15.41	1.69	5.26	0.8	4.76	0.54	9.34	0.3	0.97	0.66
4Nb	12.77	1.47	10.64	1.28	5.3	0.56	7.65	0.72	0.88	
5Nb	11.42	1.86	9.18	1.13	5.57	0.63	6.81	0.52	0.9	1.2
6Nb	12.68	1.42	8.52	1.48	6.45	0.6	6.9	1.46	0.78	
7Nb	11.62	1.7	6.32	0.89	6.99	1	6.82	1.77	0.98	1.44
9Nb	10.72	1.57	7.52	1.44	6.46	0.83	6.64	2.48	1.1	1.35
Series xNbyMg										
2Nb4Mg	14.47	2.06	6.58	1.1	4.33	0.44	7.87	0.63	1.04	1.9
3Nb2Mg	14.98	1.8	8.62	1.51	4.19	0.5	7.44	0.11	1.31	1.15
3Nb1Mg	14.01	1.94	8.19	1.59	4.91	0.37	8.18	0.17	1.39	1.11
4Nb3Mg	13.24	2.04	6.8	1.28	5.5	0.67	6.17	1.61	1.24	1.72
12Nb2Mg	12.54	2.2	6.39	1.52	5.7	1.29	6.07	3.53	1.31	1.55

[a]: $(PO_4)^{3-}$ or $(P_2O_7)^{4-}$ [27-29], [b]: P_2O_5 [29, 30], [c]: Na_3PO_4 [32], [d]: Na_2O [34], [e]:Nb_2O_5 [25], [f]: Nb^{5+} connected to PO_x [26], [g]:$Ca_3(PO_4)_2$ [31], [h]:CaO [33], [i]:$Ca(NO_3)_2$ [35], [j]:Mg metal [24], [k]: mean binding energy (eV).

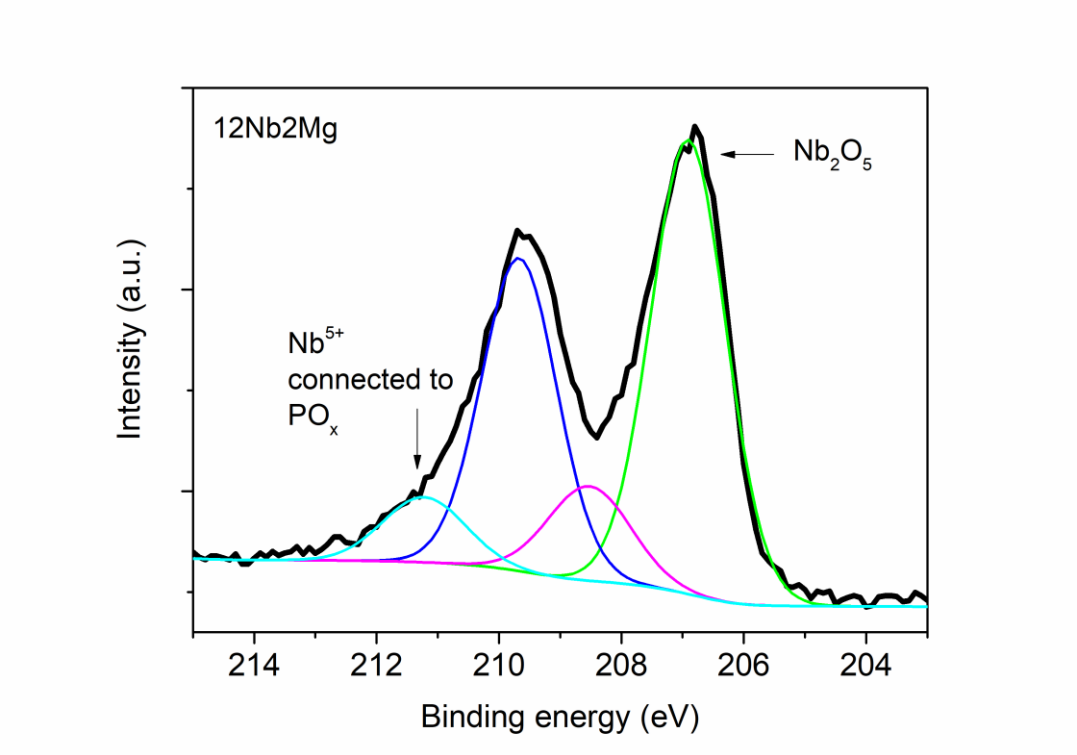

Figure 1. The exemplar XPS result of niobium fitting showed for sample 12Nb2Mg.

The topography of the cross-sections of the series Nb is shown in Fig. 2. Sample 3Nb presents homogenous morphology typical for amorphous materials. However, with the increase in Nb content, structures with different shapes and sizes can be observed. Examples of structures are marked with blue circles. The amount of visible structures increases with the Nb content. The structures indicate the partial crystallinity of samples. In addition, in the sample with the highest Nb content, the structures obtain geometrical shapes, as presented in the insert in Fig. 2 (red frame). These geometrical structures are rich in Nb, Ca, and Na while lacking in P. Figure 3 shows the topography of the series NbMg samples. Samples 2Nb4Mg, 3Nb2Mg, and 3Nb1Mg with the Nb content close to 3 at% exhibit similar topography, typical for partially crystallized glassy samples. Examples of structures are also marked with blue circles. In samples 4Nb3Mg and 12Nb2Mg, the content of visible structures increases sharply. For 4 at% of Nb, the shape of structures is more elongated and dendritic (orange circle) while for 12 at%

of Nb rounded structures were observed (green circle). These rounded structures are rich in phosphorous and calcium while lacking in the other elements.

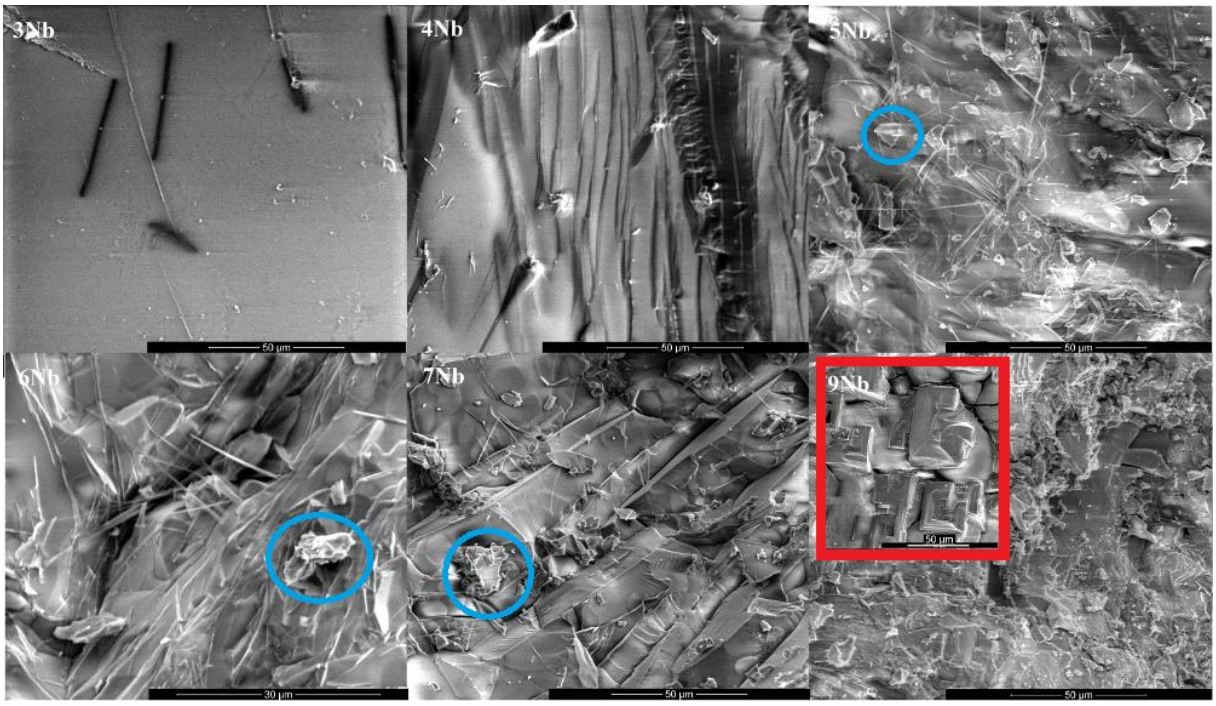

Figure 2. SEM micrographs of series Nb samples: 3Nb, 4Nb, 5Nb, 6Nb, 7Nb, and 9Nb.

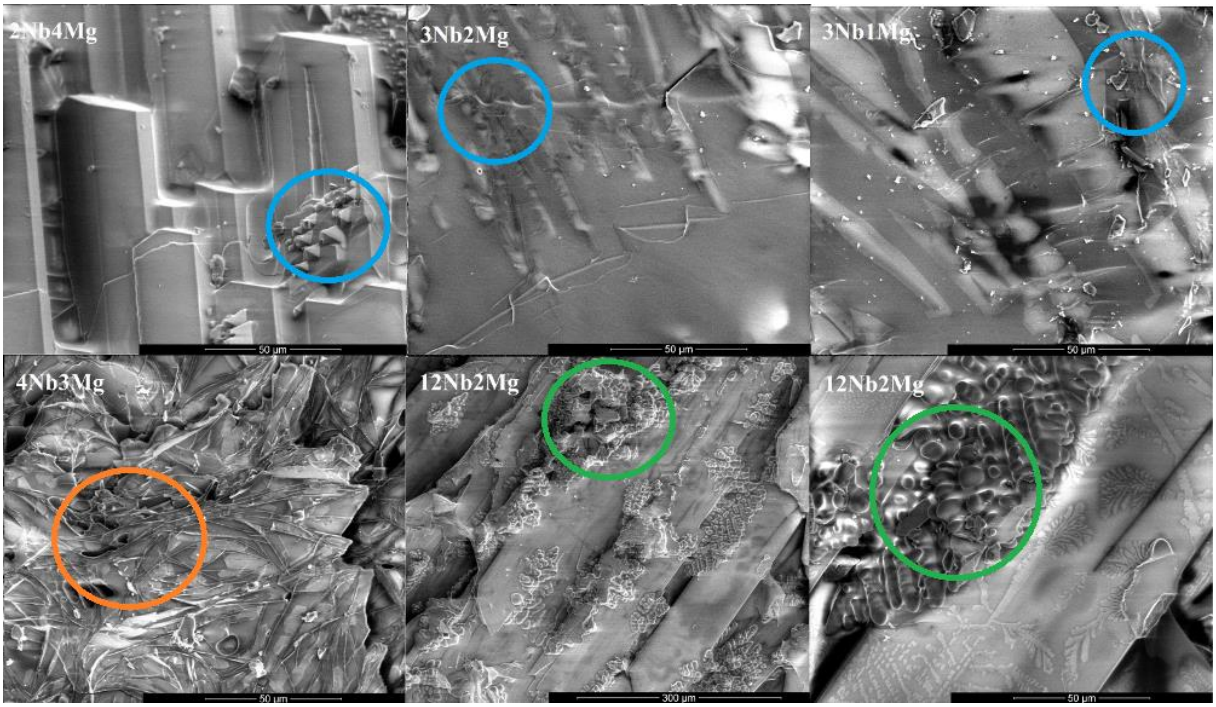

Figure 3. SEM micrographs of series NbMg samples: 2Nb4Mg, 3Nb2Mg, 3Nb1Mg, 4Nb3Mg, and 12Nb2Mg.

The XRD measurements confirm the presence of crystallinity in all samples. Figure 4a displays X-ray diffraction patterns for exemplar samples: 3Nb, 5Nb, and 7Nb. Sample 3Nb is mostly amorphous with three small and broad reflections correlated with $Ca_{2.86}Mg_{0.14}(PO_4)_2$ crystalline phase. Samples 4Nb and 5Nb have similar X-ray patterns which contain an amorphous halo and some small and broad reflections assigned to the $Ca_3(PO_4)_2$ and $Ca_9MgNa(PO_4)_7$ crystalline phases, respectively. The intensity of the three main reflections was higher in sample 5Nb than in 4Nb, suggesting a slightly higher degree of crystallinity. The X-ray pattern of sample 6Nb partially overlapped with that of 5Nb, however, the new and at the same time main reflection can be assigned to the $CaNb_2O_6$ crystalline phase. Samples 7Nb and 9Nb exhibit X-ray patterns significantly different from previously described ones 3Nb, 4Nb, and 5Nb. The observed intensive reflections are mostly correlated with the $CaNb_2O_6$ crystalline phase. Some small reflections are also assigned to $Ca_3Mg_3(PO_4)_4$ and $Ca_9MgNa(PO_4)_7$ in sample 7Nb and NaNbO in sample 9Nb. These results confirm that the crystals visible in SEM micrographs are composed only of niobates in sample 9Nb which is in accordance with EDX results. In sample 7Nb most of the crystalline phase is also made of niobates, but phosphates are also present. In Table 3, the summary of the fitted crystalline phase is listed for each sample. Scherrer equation was used to estimate the mean size of crystals for dominating reflections. Additionally, the approximate degree of crystallinity was estimated using the established relation that the percentage of crystallinity is equal to the area of crystalline reflections divided by the full area of crystalline and amorphous phases. However, the estimations could become very uncertain due to shifts and the broadening of reflections caused by the amorphous halo. Therefore, the obtained values are simply employed to enhance the considerations. The degree of crystallinity decreases, while the niobate ceases to be the dominant phase and the phosphates become the dominant one. Similar behavior is observed for the mean size of crystals in most of the samples. The one exception, sample 4Nb, which exhibits bigger crystals than other samples

containing phosphates can be correlated with the lack of Mg. It can be assumed that the addition of magnesium limits crystal growth, due to taking part in the formation of the crystals. Therefore, higher content of smaller crystals is observed in sample 5Nb. The samples in series Nb can be ranked ascendingly according to the increase in the degree of crystallinity: 3Nb < 4Nb < 5Nb < 6Nb < 7Nb < 9Nb. Analogous X-ray diffraction results were found for samples in series NbMg presented in Fig. 4b. In sample 2Nb4Mg, the reflections are mostly correlated to $Ca_9MgNa(PO_4)_7$ phase. Additionally, small reflections were found to be assigned to crystalline $CaNb_2O_6$. Samples 3Nb2Mg and 3Nb1Mg show a similar crystalline structure built of only $Ca_9MgNa(PO_4)_7$ phase. In sample 4Nb3Mg, the $CaNb_2O_6$ phase starts to be more noticeable while in sample 12Nb2Mg it is dominating. Instead of niobate, there is also calcium phosphate in a crystalline form in the 12Nb2Mg. Likewise, as in series Nb, also in series NbMg, the crystallinity degree mostly increased with the Nb content, with exception of 2Nb4Mg which contains the highest amount of Mg. Samples with the highest Mg content e.g., 2Nb4Mg, 4Nb3Mg, and 12Nb2Mg showed the highest amount of the smallest crystals from the NbMg series. It confirms the indispensable influence of magnesium on crystal growth. Furthermore, in both series in the Nb-rich samples such as 7Nb, 9Nb, and 12Nb2Mg a small reflection around 31.7^o is barely visible. This reflection can be correlated with the crystalline hydroxyapatite, $Ca_5(PO_4)_3(OH)$ (Reference code 01-089-4405, ICSD collection code: 050656).

Based on these observations, we correlated the Nb content with the partial crystallization of samples that occurred spontaneously during the melting process. It can be stated that the higher the Nb content in the sample, the stronger the tendency for the melt to crystallize. Furthermore, for the low Nb content, the crystallization process of phosphates is preferred. In the melt with more than 5.4 at % of Nb, the Nb tends to be in crystalline form. The reason can be the supersaturation of the glass melt with Nb content.

Table 3. Results estimated basis on XRD spectra: the degree of crystallinity, residual glass phase content, the chemical formula of identified crystalline phase, its reference code and ICSD collection code, and mean size of crystals estimated using Scherrer formula.

Code	Full crystalline phase content (%)	Residual glass phase content (%)	Signature and chemical formula of crystalline phase	Reference code, ICSD collection code	Mean size of crystals ±10% (nm)
Series Nb					
x ($Mg – Mg_3N_2/Ca_3N_2$) - (100 – x)($15.3Na_2O – 36.2P_2O_5 – 39.3CaO – 7.4Nb_2O_5 – 1.7Al_2O_3$) in (%mol)					
3Nb	16	84	* $Ca_{2.86}Mg_{0.14}(PO_4)_2$	01-077-0692, 041846	64
4Nb	27	73	# $Ca_3(PO_4)_2$	01-070-2065, 006191	110
5Nb	39	61	^ $Ca_9MgNa(PO_4)_7$	01-088-0797, 085108	80
6Nb	48	52	~$CaNb_2O_6$	01-071-2406, 015208	88
			^ $Ca_9MgNa(PO_4)_7$	01-088-0797, 085108	
7Nb	53	47	~$CaNb_2O_6$	01-071-2406, 015208	155
			^ $Ca_9MgNa(PO_4)_7$	01-088-0797, 085108	
			@ $Mg_3Ca_3(PO_4)_4$	01-073-1182, 023642	
9Nb*	55	45	~$CaNb_2O_6$	01-071-2406, 015208	165
			& $NaNbO_3$	01-075-2102, 031867	
			^ $Ca_9MgNa(PO_4)_7$	01-088-0797, 085108	
Series NbMg					
x ($Mg – Mg_3N_2$) - (100 – x)($14.5Na_2O$-$37.4P_2O_5$-$39.9CaO$-$3Nb_2O_5$-$3.4MgO$-$1.7Al_2O_3$) in (%mol)					
2Nb4Mg	64	36	^$Ca_9MgNa(PO_4)_7$	01-088-0797, 085108	124
			~$CaNb_2O_6$	01-071-2406, 015208	
3Nb2Mg	43	57	^$Ca_9MgNa(PO_4)_7$	01-088-0797, 085108	137
3Nb1Mg	45	55	^$Ca_9MgNa(PO_4)_7$	01-088-0797, 085108	150
	78	22	^$Ca_9MgNa(PO_4)_7$	01-088-0797, 085108	103

4Nb3Mg			~$CaNb_2O_6$	01-071-2406, 015208	
12Nb2Mg	79	21	~$CaNb_2O_6$ @ $Mg_3Ca_3(PO_4)_4$	01-071-2406, 015208 01-073-1182, 023642	111

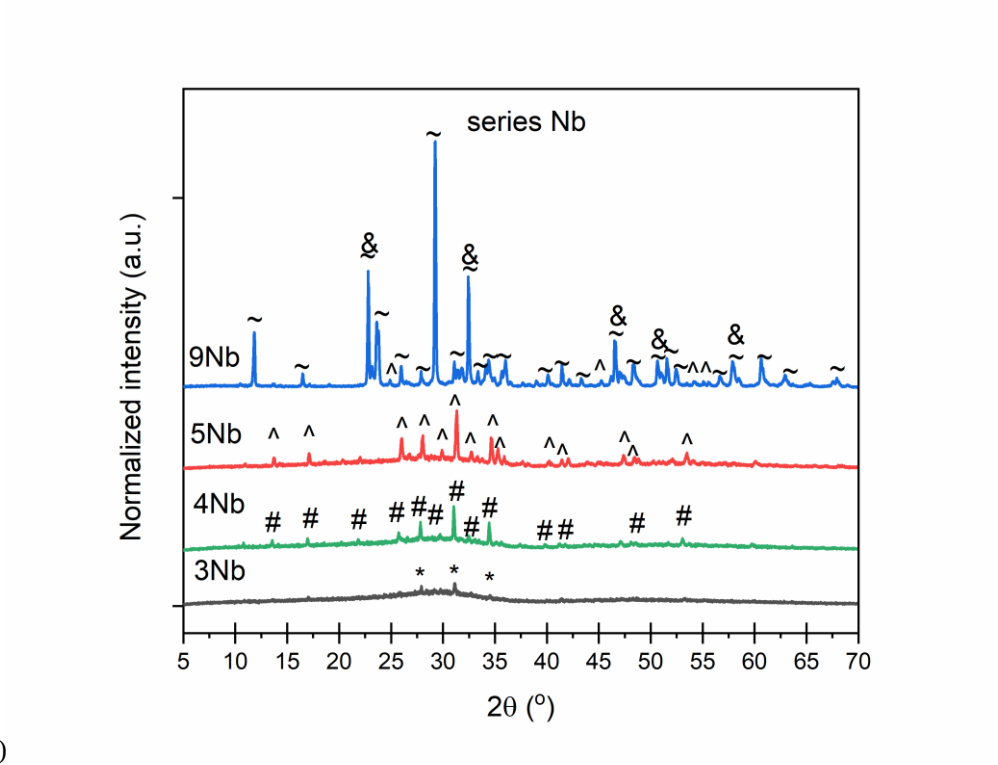

a)

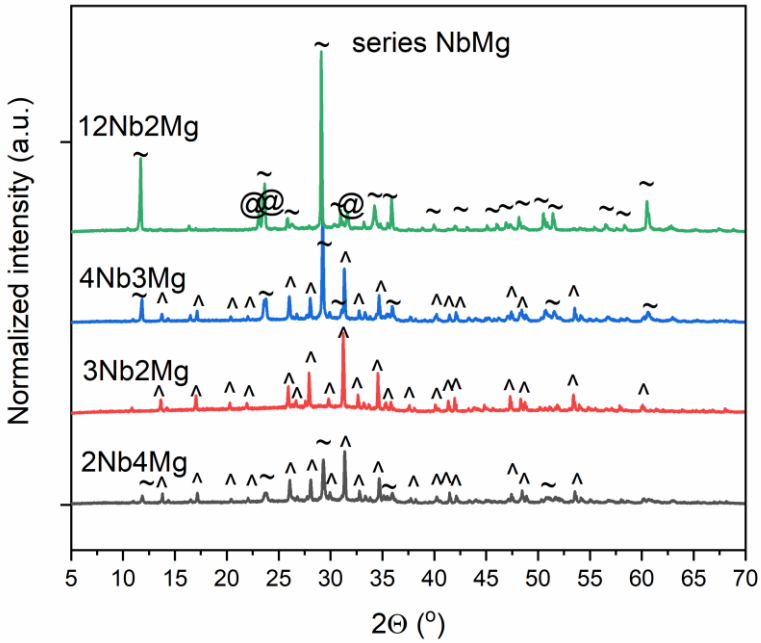

b)

Figure 4. XRD results for exemplary samples from series a) Nb and b) NbMg. The designations are correlated with crystalline phases listed in Tab. 3.

Figure 5 shows the FTIR spectra of all samples. The observed FTIR bands are mainly due to the phosphate network, which occurs in the range of 400-1500 cm^{-1}. Sample 3Nb showed the rounded shapes of curves bands indicating the amorphous nature while the other samples showed sharpened bands typical for the crystalline phase. The structural changes caused by re-melting with Mg and Mg_3N_2/Ca_3N_2 are investigated by comparing the base Na-Ca-Nb-P-O glass (0Nb) and sample 3Nb as shown in Fig. 5a. The FTIR spectrum of sample 0Nb was described in our previous paper [13] and here only a brief summary will be given. The FTIR spectra of both samples show some similarities in characteristic bands' positions. Sample 0Nb has an O:(P+Nb) ratio close to 3.2, indicating a structure consisting of 50 % of the Q^2 units and 50 % of the Q^1 units (Q^n denotes a phosphate tetrahedral unit with *n* bridging and *4-n* terminal oxygen atoms). The FTIR spectrum of the 0Nb sample shows main bands at 1166 cm^{-1}, 1088 cm^{-1}, and ~915 cm^{-1} which are due to the symmetric stretching vibration of the terminal PO_2^-

groups, $_{vs}(PO_2^-)$, of Q^2 units, and the asymmetric stretching vibration of P-O-P bridges of the Q^1 group ($_{vas}$(P-O-P)) [36-40]. The main band is asymmetrical and contains a small shoulder at ~981 cm^{-1} which can be assigned to the asymmetric stretching vibration of the Q^0 unit ($_{vas}(PO_4)^{3-}$) [41]. The presence of the Q^0 unit resulted from Q^1 site disproportionation reactions that occurred during the reorganization of the glass liquid $2Q^1 = Q^2 + Q^0$ [42]. The next small band occurred at ~735 cm^{-1} and is correlated with the symmetric stretching vibrations of P-O-P linkages, ($_{vs}$(P-O-P)), in Q^1 units [41]. The highly pronounced band found at ~560 cm^{-1} can be assigned to $_v$(P-O) bonding in $(PO_4)^{3-}$ [43] or the vibrational coupling of [$_v$(Nb-O) (medium Nb-O distances) (O-P-O)] stretching with deformation modes [42]. Additionally, a small shoulder occurred at ~638 cm^{-1} which can be correlated with the asymmetric stretching vibration of the Nb-O-Nb bridges of distorted NbO_6 octahedra $_{vas}$(Nb-O) [42]. Sample 3Nb was prepared through doping glass 0Nb with Mg and Ca which should cause depolymerization of the phosphate network. The O:(P+Nb) ratio for sample 3Nb with a value 3.4 also suggests higher content of Q^1 units instead of Q^2 units. Consequently, the main band in its FTIR spectrum was observed at 1061 cm^{-1} with a second band of lower intensity at ~1120 cm^{-1}, the changes in the relative intensity and movement of bands into lower frequencies suggest a decrease in the Q^2 and an increase in Q^1 units contents and consequently a more depolymerized structure than in glass 0Nb. At the same time, a band at 985 cm^{-1} correlated with the Q^0 units is more pronounced in sample 3Nb. Moreover, the bands at ~630 and 548 cm^{-1} exhibit a higher relative intensity suggesting highlighting the Nb role in the glass network as well as the presence of Q^0 phosphate units which is in accordance with the XPS results. Therefore, we can conclude that niobate groups occurred in the form of NbO_6 units in this glass system similar to parent 0Nb glass. Additionally, a small envelope was observed at 589 cm^{-1} which can be correlated with the presence of the nanocrystalline phosphates phase [44, 45] which was also found in XRD analysis.

The other samples in series Nb show significant changes in FTIR spectra compared to sample 3Nb, as shown in fig. 5b. In sample 4Nb the main band correlated with Q^1 units is shifted towards lower wavenumbers ~1038 cm^{-1} while a band of Q^2 units at ~946 cm^{-1} is significantly lower in intensity than in sample 3Nb both indicate slightly higher depolymerization of the phosphate network. It can be due to the increase in the content of sodium ions which are known as a network modifier and at the same time decrease in the content of phosphorous which is a glass former. Moreover, the bands correlated with the Q^0 units at ~975, ~587, and ~546 cm^{-1} are more pronounced and sharpened, indicating the occurrence of PO_4^{3-} in crystal form. Most likely, crystals are of nanometer size. However, Nb content increases in this sample while its effect is the opposite in the phosphate network, it should increase the polymerization. Consequently, the small envelope is visible at ~895 cm^{-1} which is due to the asymmetric stretching vibration of group Q^2. The band at 645 cm^{-1} which indicates the Nb presence in NbO_6 units, is barely visible due to high overlapping with the neighboring band, however band at 546 cm^{-1} can also be assigned to the O-Nb band. The FTIR spectrum of sample 5Nb shows more pronounced and sharpened bands than in sample 3Nb however in similar positions. Especially the main changes are visible in dominating bands indicating the higher content and size of the crystalline phase built of phosphates. The FTIR spectrum for 6Nb partially overlaps with 5Nb. For the 6Nb sample, XRD data indicated one of the crystalline phases as $CaNb_2O_6$, which displays dominating bands in the FTIR spectrum at 497, 550, 747, 805, and 867 cm^{-1}. In the FTIR spectrum of the 6Nb sample, it is possible to distinguish some sharp bands at 882, 730, 469, and 431 cm^{-1}. We correlate them with an increase in niobium content in the sample and consequently the occurrence of a new crystalline phase built of niobates. The new bands observed for sample 6Nb are typical for the coupled modes O–Nb and O–Nb–O–P. The further increase in Nb content caused significant changes in the structure of sample 7Nb. The positions and relative intensity of bands indicate that the glass network is built

of Q^2, Q^1, and Q^0 units. The intensity of sharpened bands in the low-frequency region significantly increases due to an increase in the crystalline phase content. Taking into account also the XRD results, it can be stated that in sample 7Nb the band at 550 cm^{-1} is correlated with niobates crystals [16]. Additionally, the FTIR results also confirm the presence of phosphate crystals [44, 45]. In the 9Nb sample with the highest content of Nb, the FTIR spectrum has the main band at ~1040 cm^{-1} which is due to Q^1 units occurrence. At the same time, the sharp band at ~570 cm^{-1} is the second dominating one which is in accordance with the high content of niobate crystals. In addition, high content of Q^0 units is found, which is confirmed by the intensive band at ~600 cm^{-1}. The observed decrease in the intensity of the bands in the region from 830 to 900 cm^{-1} is correlated with the decrease in the content of Q^2 units. All these features suggest the increase in depolymerization of the glass network. This is due to the fact that the niobium is not only incorporated into the phosphate glass network but is mainly involved in crystals formation. The FTIR spectra for series NbMg are displayed in fig. 5c. High similarities are observed between FTIR spectra of the samples 2Nb4Mg, 3Nb2Mg, 3Nb1Mg, and 4Nb3Mg, which are also in good agreement with the spectrum of sample 5Nb. However, in the NbMg series, most of the bands are more sharpened than in sample 5Nb, suggesting higher content of crystallinity built up of phosphates. In samples 2Nb4Mg and 4Nb3Mg, the clearly visible bands at 887, 740, 476, and 430 cm^{-1} confirmed the presence of niobate in crystalline form which is in consistent with XRD results. Interestingly, instead of low Nb content, sample 2Nb4Mg contains niobate crystals while samples 3Nb2Mg and 3Nb1Mg with higher Nb content do not show the evidence for it. The reason is probably the higher Mg content in 2Nb4Mg sample which can support the niobate crystallization process. The Mg effect can also be observed when comparing the FTIR spectra of samples 3Nb1Mg and 3Nb2Mg. In 3Nb2Mg sample with a higher Mg content, the shoulder around 880 cm^{-1} and small band at 740 cm^{-1} can be distinguished, indicating the possible beginning of the niobate crystallization process. The FTIR

spectrum of the 12Nb2Mg sample is close to the ones of the 7Nb and 9Nb samples in which the $CaNb_2O_6$ is the predominant crystalline phase. Since the $CaNb_2O_6$ crystal is composed of CaO_6 and NbO_6 octahedra, therefore NbO_6 is the most dominant form of niobate groups even in glass-ceramics.

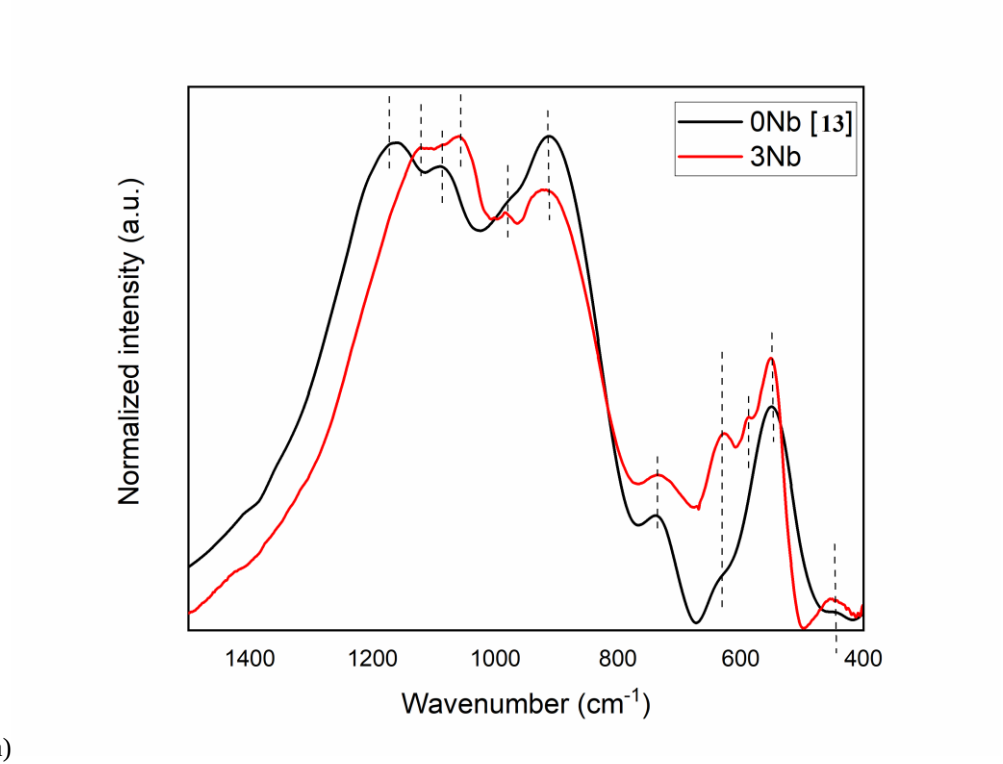

a)

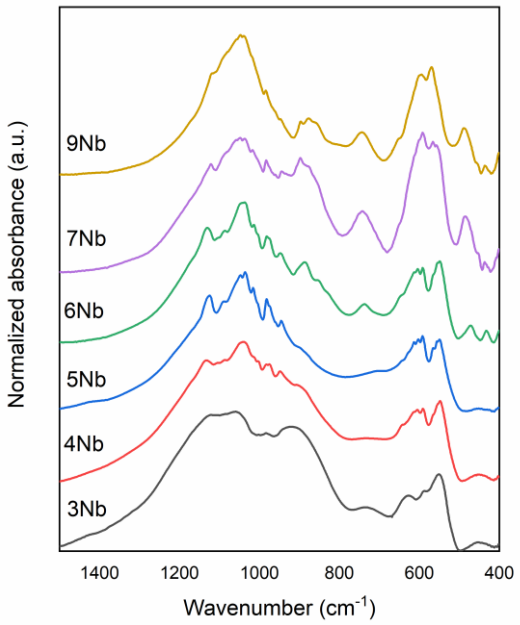

b)

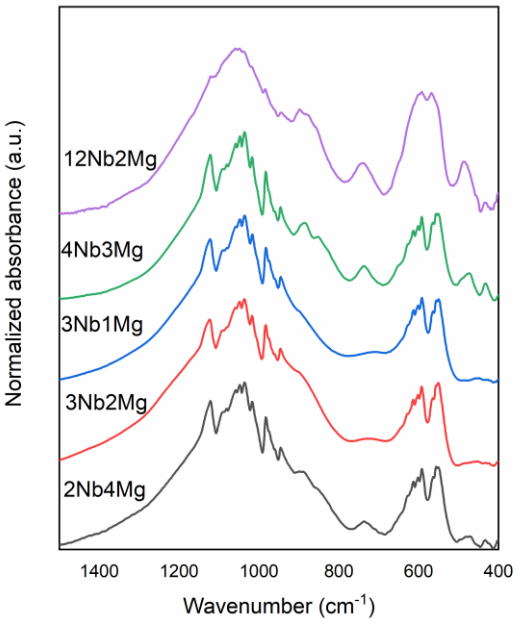

c)

Figure 5. The comparison of FTIR spectra for samples: a) 0Nb ([13]) and 3Nb, b) series Nb and c) series NbMg. Spectra were background corrected and normalized.

3.2. Thermal properties

The glass transition temperature as a function of Nb content is shown in 6a & 6b for series Nb and NbMg, respectively. The T_g was only possible to estimate for samples with a nanocrystalline phase (c.f., table 4). For samples 7Nb, 9Nb, and 12Nb2Mg which have microcrystallites, the T_g was not possible to be correctly detected. Thermal properties exhibit strong dependence on the Nb amount and the degree of crystallinity, see tables 3 and 4. It is known that the increase in Nb content increases the T_g of phosphate base glasses, due to the increase of network polymerization by Nb addition [13-16]. This correlation was observed for the NbMg series (fig. 6b). However, in series Nb the T_g dependence was the opposite. In the Nb series, with the increase of the Nb content, the content of phosphorous decreased. In addition, the glass transition refers only to the residual glass matrix in which the crystals are distributed. Therefore, a decrease in the T_g was observed with the increase in the content of the phosphate crystalline phase. The more phosphorous is involved in the formation of the phosphate crystals, the less of it can build up the residual glass network. Then the remaining niobate-phosphate glass network doped with modifiers is more depolymerized and shows lower T_g. A similar trend in the network polymerization degree with the increase of phosphate crystals content is in accordance with the FTIR results. In the series NbMg, high content of phosphate is trapped in crystallites and does not build the glass network, however, concurrently niobium is also partially in crystalline form. Moreover, the Mg which is in higher content in these samples can also increase the T_g. Therefore, the increase in T_g is a combined effect. Besides significantly different structures all samples in series NbMg exhibit the improvement of glass transition temperature through re-melting compared to target glass 0MgNb.

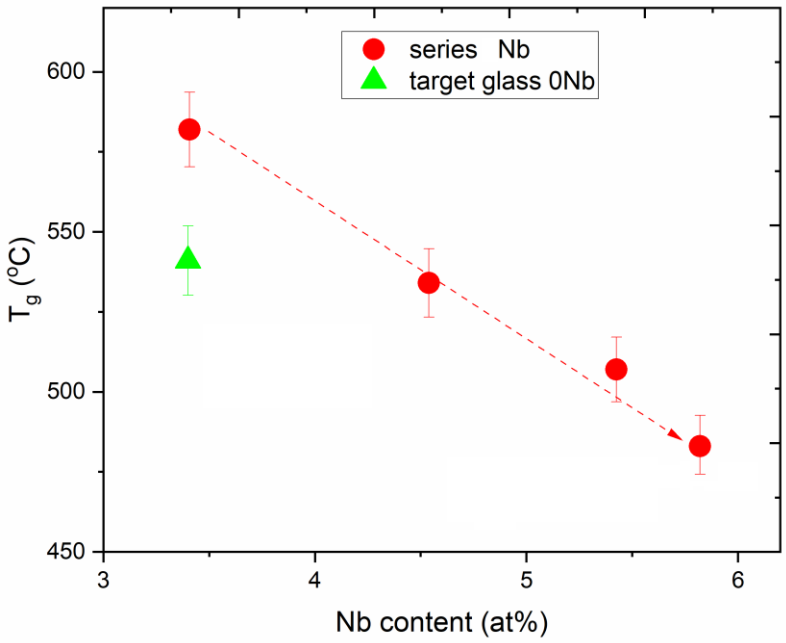

a)

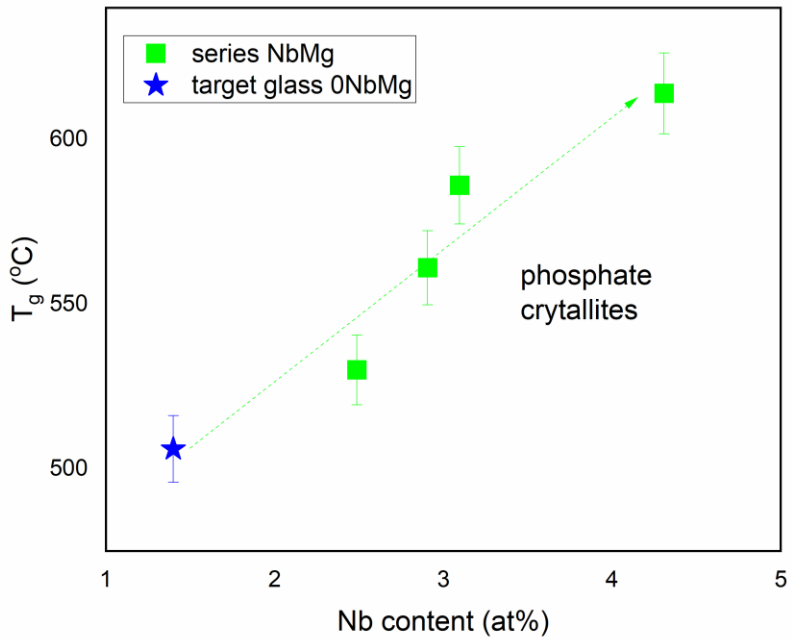

b)

Figure 6. T_g as a function of Nb content for a) series Nb samples containing phosphate crystals and for b) series NbMg samples. Mention that the dot-line is only for eye guidance.

Table 4 shows the thermal parameters evaluated for all samples. Glass thermal stability was estimated as $S = T_{cr\ onset} - T_g$ where $T_{cr\ onset}$ is the beginning of the crystallization process (observed at the DSC curve as an exothermic process) [46-48]. The clear correlation between thermal stability and an increase in Nb content is visible for samples: 3Nb, 4Nb, 5Nb, and 6Nb, containing phosphate nanocrystals. The target glass 0Nb exhibits a thermal stability value of 150 ^oC while for 0NbMg is around 135 ^oC [13]. Almost all prepared glass-ceramic composites have significantly higher thermal stability than base glasses. Among the different samples, 6Nb containing both phosphate and niobate crystals had the highest thermal stability values (298 ^oC).

Table 4. Thermal properties: glass transition temperature T_g, crystallization process parameters $T_{cr\ onset}$ and $T_{cr\ peak}$, and glass thermal stability S. All parameters are given with the accuracy ± 2%.

Sample code	T_g (^oC)	$T_{cr\ onset}$ (^oC)	$T_{cr\ peak}$ (^oC)	S (^oC)
		Series Nb		
3Nb	582	693	746	111
4Nb	534	804	829	270
5Nb	507	782	835	275
6Nb	483	781	813	298
7Nb		794	891	
9Nb		794	807	
		Series NbMg		
2Nb4Mg	530	864	878	162
3Nb2Mg	561	751	844	269
3Nb1Mg	586	727	803	141
4Nb3Mg	614	736	747	122
12Nb2Mg		861	878	

3.1. In vitro dissolution in PBS

The *in vitro* dissolution tests were carried out in PBS for 6 and 13 days and obtained mass losses are listed in Table 5. It is evident that the highest mass loss occurred during the first 6 days of immersion in most of the samples. The presence of crystalline calcium phosphates in samples 4Nb and 5Nb slows down the dissolution slightly, while crystalline niobates support the dissolution process. It might be due to the fact that PBS contains phosphorous and lacks niobium, and the solution tends to level this disproportion. In a long-term immersion i.e., 13 days, this trend is not clearly visible. Most probably this is due to the saturation of PBS with the niobium. Sample 3Nb which is mostly amorphous shows also quite a high mass loss. The mass loss for sample 4Nb after long-term incubation is only 1.1 and it is significantly lower than the initial value. This inconsistence might be due to the fact the powders of sample 4Nb after long-term incubation were not dried completely and a small amount of water – imperceptible to the naked eye – may increase mass. The other possibility is that the dissolution process slowed down after 6 days and the increase in mass was caused by the build-up of the hydroxyapatite layer on the surface. It is known that to increase the supersaturation of hydroxyapatite in PBS, a number of calcium ions should release from the materials. In our previous paper [13] the Ca ions releasing effect was confirmed for parent glasses 0Nb, 0NbMg and we assumed that it also proceeds for tested glass-ceramics. In that case, we can suggest that in sample 4Nb the release process of Ca ions into PBS was more effective than the one of P ions as PBS is already saturated in it. Then hydroxyapatite formation is set between P ions occurring in PBS and Ca ions originating from the material. Unlike other samples, this behavior is only noticeable in 4Nb, due to lack of Mg and crystals are built of $Ca_3(PO_4)_2$. Ordering the samples according to Mg content, we get 6Nb<3Nb<5Nb<9Nb<7Nb and a similar tendency can be found for mass loss after long-term immersion. Mg, like Nb, can be regarded as a

dissolution accelerator because of its absence in PBS. Sample 7Nb showed slightly lower mass loss than 9Nb instead of a higher Mg amount. However, in this sample some of Mg ions are incorporated into $Mg_3Ca_3(PO_4)_4$ crystals are less dissolve than the calcium-richer $Ca_9MgNa(PO_4)_7$ crystals that occurred in other samples. For series NbMg the Mg influence is noticeable already for the initial stage of immersion 3Nb1Mg<3Nb2Mg<4Nb3Mg<2Nb4Mg. In this case, sample 12Nb2Mg deviates from the trend because it also contains $Ca_9MgNa(PO_4)_7$ crystals.

The pH changes during the immersion process were small, indicating the uniform dissolution process. The highest increase in pH was observed during the first day. In sample 4Nb the change was 0.1 and for sample 9Nb it was 0.09. However, the pH of PBS slightly increases during the entire immersion suggesting the continuous dissolution process for each sample. The total pH changes counted for all measurements were the most noticeable for samples 7Nb and 9Nb which is in accordance with the highest mass loss. The increase in pH can be due to the dissolution of Na^+, Ca^{2+}, Mg^{2+}, and Nb^{5+} ions while the dissolution of P^{5+} will acidify the solution [13, 19, 49].

Table 5. The mass loss of glasses after immersion in PBS for 6 and 13 days, the ratio of crystallinity degree after 6 or 13 days of immersion to starting one.

Step of immersion	Immersion time (days)	Series Nb					
		3Nb	4Nb	5Nb	6Nb	7Nb	9Nb
		Mass loss after immersion in PBS (%)					
Initial stage	6	9.6	5.3	6.1	8.3	9.1	10.9
Long term	13	11.2	1.1	12.4	10.2	17.0	17.5
		The ratio of crystallinity degree after 6 or 13 days of immersion to starting one					

Initial stage	6	$\frac{12}{16}$	$\frac{26}{27}$	$\frac{34}{39}$	$\frac{35}{48}$	$\frac{46}{53}$	$\frac{39}{55}$
Long term	13	$\frac{13}{16}$	$\frac{20}{27}$	$\frac{25}{39}$	$\frac{35}{48}$	$\frac{40}{53}$	$\frac{35}{55}$
				Series NbMg			
		2Nb4Mg	3Nb2Mg	3Nb1Mg	4Nb3Mg	12Nb2Mg	
				Mass loss after immersion in PBS (%)			
Initial stage	6	11.0	9.7	7.8	9.7	11.5	
Long term	13	11.3	6.3	13.5	8.6	15.3	
		The ratio of crystallinity degree after 6 or 13 days of immersion to starting one					
Initial stage	6	$\frac{56}{64}$	$\frac{33}{43}$	$\frac{35}{45}$	$\frac{45}{78}$	$\frac{44}{79}$	
Long term	13	$\frac{40}{64}$	$\frac{37}{43}$	$\frac{37}{45}$	$\frac{30}{78}$	$\frac{47}{79}$	

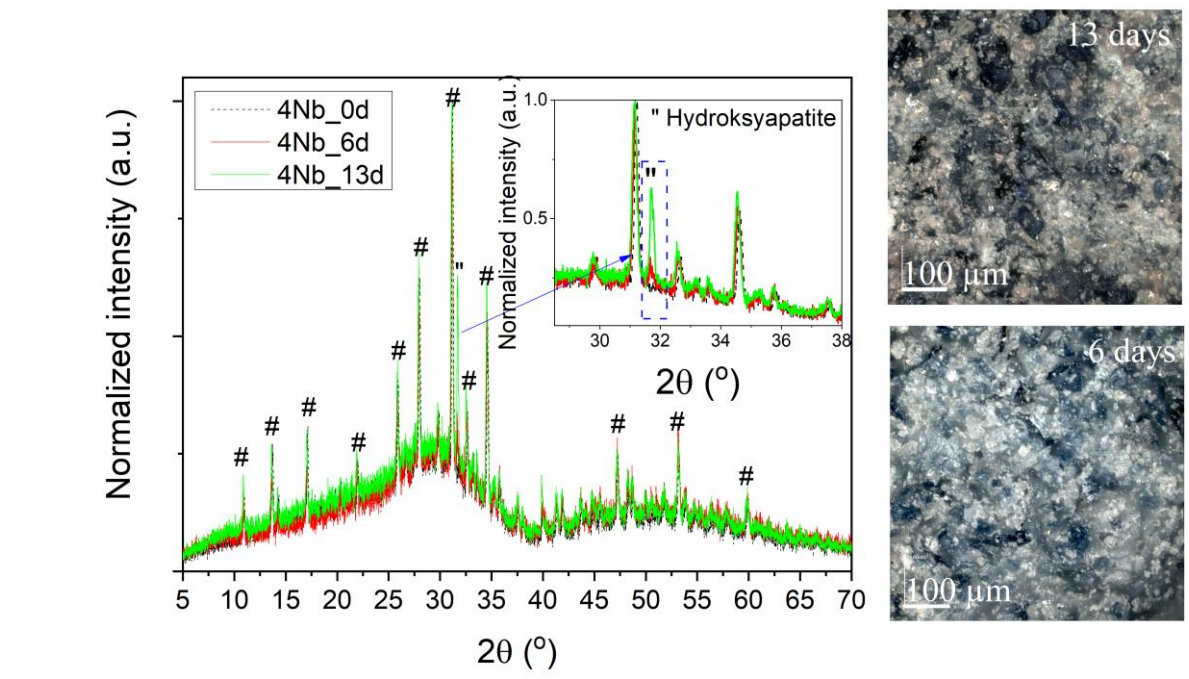

Figure 7. X-ray diffractions for exemplar sample 4Nb after 6 and 13 days of immersion in PBS. On the right, are the confocal microscope micrographs of sample 4Nb after 13 and 6 days of immersion.

The XRD measurements of powdered samples were performed after immersion in PBS for 6 and 13 days. The X-ray analysis showed that the structural changes occurred in all samples through the dissolution or precipitation process. In most samples 3Nb, 4Nb, 6Nb, 3Nb2Mg, 3Nb1Mg, and 4Nb3Mg new reflection close to 31.7^{o} assigned to the crystalline hydroxyapatite was observed. This reflection is of low intensity after 6 days of immersion and through further incubation, it starts to be dominating one (shown in fig. 7 and marked by a blue frame in the inset). The obtained results are incontrovertible evidence of the deposition of crystalline hydroxyapatite on tested powders. In samples 7Nb, 9Nb, and 12Nb2Mg the HAp phase was noticeable before and after the *in vitro* dissolution test. Therefore, the origin of HAp reflection visible for their XRD data after immersion is not unequivocal. It is certain that HAp crystals formed during the melting/cooling process, however, we cannot rule out the possibility of the dissolution and deposition processes of HAp during immersion. Only samples 5Nb and 2Nb4Mg do not show evidence of the presence of HAp in their X-ray diffractions after immersion. In our previous study describing the parent 0Nb, 0NbMg glasses [13], we observed that the Mg visibly escapes from the phosphate structure as well as supports the effect on Nb escaping. Even though the 2Nb4Mg sample has the highest amount of Mg, the process of Nb and Mg ions release is predominant and thus inhibits the deposition of HAp on the surface.

In samples 9Nb and 12Nb2Mg, the immersion caused also high changes in the intensity of dominating reflections. The normalized intensity of dominating reflections visibly decreased after 6 days and further decreased after the next 7 days of immersion. These observations indicate the dissolution process of the calcium niobate crystalline phase found in samples and an increase in the content of the amorphous phase. In sample 9Nb the dissolution process of sodium niobate was also observed after the first 6 days of immersion. To check the approximate magnitude of visible changes, the ratio of crystallinity degree after immersion to the starting one was estimated and is listed in Tab. 5 for all samples. It can be seen that the degree of

crystallinity decreases after immersion in all glass-ceramics. The largest changes were observed for materials Nb- and/or Mg-rich containing niobate crystals e.g., samples 4Nb3Mg, 12Nb2Mg, 2Nb4Mg, and 9Nb. However, the results are only an approximation with variations of up to 5% uncertainty. Furthermore, for most of the samples, a high decrease in percentage crystallinity confirms the dissolution process of crystals. Additionally, the mean size of crystals was estimated after 6 and 13 days of immersion but no significant changes were noticed. From these observations, it can be concluded that the dissolution process occurred mostly on the surface of powders granules and refers to crystals in contact with a solution.

The dissolution process proceeds not only through the ions released into PBS but also through the deposition process as mentioned before. Consequently, a new HAp layer formed on the powdered samples as confirmed by XRD results. The exemplary micrographs of the layer are shown for sample 4Nb after 6 and 13 days of immersion, Fig. 7 right. EDX measurements were done for powders after 13 days of immersion in PBS. The obtained compositions were close to the ones before immersion however, small changes were also detected for all samples. In samples 7Nb, 9Nb, and 12Nb2Mg the content of Nb decreased confirming the dissolution process of niobates. In the other samples, the variation of Na, Ca, Mg, and P contents were between 1 - 2 at% and give the Ca/P ratio mostly higher than before the immersion and close to 1, suggesting that the precipitated layers are built of phosphates. In all samples, a trace amount of Cl was also detected which comes from the PBS.

4. Conclusions

We have explored the effect of crystallinity on structural, thermal, and *in vitro* dissolution of bioactive glasses/glass-ceramics in the Na_2O-CaO-Nb_2O_5/MgO-P_2O_5 system prepared by a spontaneous crystallization process. The Nb content in the glass network is directly correlated to the synthesis temperature and the crystallinity increases with the increase in the Nb content. The XPS spectra manifest clear signatures of Nb_2O_5 and Mg in the glass network, which

increase accordingly to compositions. The XRD and FTIR analysis indicate that niobate crystals showed greater growth than phosphate crystals. The glass transition temperature is influenced by both the Mg, which acts as a network modifier, and Nb, which acts as a network former. The *in vitro* dissolution results show that bigger niobate crystals dissolve more readily in comparison with the smaller crystals of phosphates in PBS. However, the presence of high Nb and Mg contents does not favor the deposition of hydroxyapatite on the glass-ceramics surface.

5. Acknowledgments

We want to thank Dr. Kacper Jurak for the XPS measurements. This work was supported by the Gdańsk University of Technology [grant number DEC-19/2020/IDUB/I.3.3] under the ARGENTUM TRIGGERING RESEARCH GRANTS - 'Excellence Initiative - Research University program.

6. Statement of contribution

NAW – Conceptualization; Data curation; Formal analysis; Funding acquisition; Investigation; Methodology; Project administration; Supervision; Writing - original draft; SW - Investigation; Methodology; JLK – Methodology; Writing - review & editing; JR - Methodology; Writing - review & editing; SA – Supervision; Writing - review & editing.

7. Data availability

The data that support the findings of this study are available from the corresponding author upon reasonable request.

References

[1] J.R. Jones, P. Sepulveda, L.L. Hench, Dose-dependent behavior of bioactive glass dissolution, J. Biomed. Mater. Res. 58 (6) (2001) 720–726, https://doi.org/10.1002/jbm.10053

[2] D. Ehrt, P. Ebeling, U. Natura, UV Transmission and radiation-induced defects in phosphate and fluoride–phosphate glasses, J. Non. Cryst. Solids 263-264 (2000) 240–250, https://doi.org/10.1016/S0022-3093(99)00681-X.

[3] D. Ehrt, REVIEW: phosphate and fluoride phosphate optical glasses – properties, structure and applications, Phys. Chem. Glass. Eur. J. Glass Sci. Technol. Part B 56 (6) (2015) 217–234, https://doi.org/10.13036/17533562.56.6.217

[4] R. K. Brow, Review: The Structure of Simple Phosphate Glasses, Journal of Non-Crystalline Solids 263-264(1) (2000) 1-28. DOI: 10.1016/S0022-3093(99)00620-1

[5] L.L. Hench, R.J. Splinter, W.C. Allen, T.K. Greenlee, Bonding mechanisms at the interface of ceramic prosthetic materials. J Biomed Mater Res 1971, 5, 117–141, doi:10.1002/jbm.820050611

[6] J. R. Jones, Review of bioactive glass: From Hench to hybrids, Acta Biomaterialia 9 (1) (2013) 4457-4486, https://doi.org/10.1016/j.actbio.2012.08.023

[7] Md Towhidul Islam, Reda M Felfel, Ensanya A Abou Neel, David M Grant, Ifty Ahmed, Kazi M Zakir Hossain, Bioactive calcium phosphate-based glasses and ceramics and their biomedical applications: A review, Journal of Tissue Engineering 8 (2017) https://doi.org/10.1177/2041731417719170

[8] E.A. Abou Neel, D.M. Pickup, S.P. Valappil, R.J. Newport, J.C. Knowles, Bioactive functional materials: a perspective on phosphate-based glasses, J. Mater. Chem. 19 (2009) 690–701.

[9] I. Ahmed, M. Lewis, I. Olsen, J.C. Knowles, Phosphate glasses for tissue engineering: Part 1. Processing and characterization of a ternary-based P_2O_5-CaO-Na_2O glass system. Biomaterials 2004, 25, 491–499, doi:10.1016/s0142-9612(03)00546-5.

[10] I. Ahmed, M. Lewis, I. Olsen, J.C. Knowles, Phosphate glasses for tissue engineering: Part 2. Processing and characterization of a ternary-based P_2O_5-CaO-Na_2O glass fibre system. Biomaterials 2004, 25, 501–507, doi:10.1016/s0142-9612(03)00547-7.

[11] K. Franks, I. Abrahams, G. Georgiou, J.C. Knowles, Investigation of thermal parameters and crytallisation in a ternary CaO-Na_2O-P_2O_5-based glass system. Biomaterials 2001, 22, 497–501, doi:10.1016/s0142-9612(00)00207-6

[12] M. Uo, M. Mizuno, Y. Kuboki, A. Makishima, F. Watari, Properties and cytotoxicity of water soluble Na_2O-CaO-P_2O_5 glasses. Biomaterials 1998, 19, 2277–2284, doi:10.1016/s0142-9612(98)00136-7

[13] N. A. Wójcik, S. Wolff, J. L. Karczewski, M. Rutkowska, S. Ali, Effect of Nb and Al on in vitro dissolution behavior and structure of Na_2O-MgO–CaO-P_2O_5 glasses. Journal of Non-Crystalline Solids 585 (2022) 121544, https://doi.org/10.1016/j.jnoncrysol.2022.121544

[14] N. A. Wójcik, S. Ali, E. I. Kamitsos, D. Möncke, Niobate in silicate and phosphate glasses: Effect of glass basicity on crucible dissolution. Int J Apl Glass Sci. 13 (2022) 121-134. DOI: 10.1111/ijag.16505

[15] Wójcik, N.A.; Jonson, B.; Möncke, D.; Palles, D.; Kamitsos, E.I.; Ghassemali, E.; Seifeddine, S.; Eriksson, M.; Ali, S. Influence of synthesis conditions on glass formation, structure and thermal properties in the Na_2O-CaO-P_2O_5 system doped with Si_3N_4 and Mg. J. Non-Cryst. Solids 494 (2018) 66–77, https://doi.org/10.1016/j.jnoncrysol.2018.04.055.

[16] H. Maeda, T. Miyajima, S. Lee, A. Obata, K. Ueda, T. Narushima, T. Kasuga, Preparation of calcium pyrophosphate glass ceramics containing Nb_2O_5. J. Ceram. Soc. Jpn. 2014, 122, 122–124, doi:10.2109/jcersj2.122.122.

[17] A. Obata, Y. Takahashi, T. Miyajima, K. Ueda, T. Narushima, T. Kasuga, Effects of Niobium Ions Released from Calcium Phosphate Invert Glasses Containing Nb_2O_5 on Osteoblast-Like Cell Functions. ACS Appl. Mater. Interfaces 2012, 4, 5684–5690,

doi:10.1021/am301614a.

[18] N. A. Wójcik, S. Ali, A. Mielewczyk-Gryń, B. Jonson: Two-step synthesis of niobium doped Na–Ca–(Mg)–P–Si–O glasses. Journal of Material Science 56 (2021) pages 7613–7625.

[19] N. A. Wójcik, P. Sinitsyna, S. Ali, L. Hupa, B. Jonson: In vitro dissolution of Na-Ca-P-oxy nitrides. Materials 14 (2021) 7425.

[20] Y. Zhou, H. Li, K. Lin, W. Zhai, W. Gu, J. Chang, Effect of heat treatment on the properties of SiO_2–CaO–MgO–P_2O_5 bioactive glasses, J Mater Sci: Mater Med (2012) 23:2101–2108, DOI 10.1007/s10856-012-4699-y

[21] N.A. Wójcik, N.S. Tagiara, S. Ali, K. Górnicka, H. Segawa, T. Klimczuk, B. Jonson, D. Möncke, E.I. Kamitsos: Structure and magnetic properties of BeO-Fe_2O_3-Al_2O_3-TeO_2 glass-ceramic composites. Journal of European Ceramic Society 41 (10) (2021) 5214-5222.

[22] S. Ali, A. S. Hakeem, M. Eriksson, N. A. Wójcik: A novel approach for processing CaAlSiON glass-ceramics by spark plasma sintering: mechanical and electrical properties. Journal of European Ceramic Society 42(1) (2022) 96-104.

[23] D. R. Glasson, S. A. A. Jayaweera, Formation and reactivity of nitrides II.† Calcium and magnesium nitrides and calcium cyanamide, Journal of Applied Chemistry 18 (1968) 77-83. https://doi.org/10.1002/jctb.5010180302

[24] J. Ryl, J. Wysocka, M. Jarzynka, A. Zieliński, J. Orlikowski, K. Darowicki, Effect of native air-formed oxidation on the corrosion behavior of AA 7075 aluminum alloys, Corrosion Science 87 (2014) 150-155. https://doi.org/10.1016/j.corsci.2014.06.022

[25] N. Özer, D.-G. Chen, C. M. Lampert, Preparation and properties of spin-coated Nb_2O_5 films by the sol-gel process for electrochromic applications, Thin Solid Films 277 (1996) 162, https://doi.org/10.1016/0040-6090(95)08011-2

[26] A.M. Davies, Selective Oxidation and Oxidative Dehydrogenation Reactions Using Niobium Based Catalysts, School of Chemistry, Cardiff University, Published 2009 by ProQuest LLC 2013, UMI Number: U585271, ISNI: 0000 0001 2417 4863, Thesis (Ph.D.)

[27] K. S. Siow, L. Britcher, S. Kumar, H.J. Griesser, XPS Study of Sulfur and Phosphorus Compounds with Different Oxidation States, Sains Malaysiana 47(8)(2018): 1913–1922 http://dx.doi.org/10.17576/jsm-2018-4708-33

[28] M. Pelavin, D. Hendrickson, J. Hollander, W. Jolly, Phosphorus 2p electron binding energies. Correlation with extended Hueckel charges, J. Phys. Chem. 74 (5) (1970) 1116.

[29] A. Majjane, A. Chahine, M. Et-tabirou, B. Echchahed, T. Do, P. Mc Breend, X-ray photoelectron spectroscopy (XPS) and FTIR studies of vanadium barium phosphate glasses, Materials Chemistry and Physics 143 (2014) 779-787. https://doi.org/10.1016/j.matchemphys.2013.10.013

[30] V. Simon, D. Muresan, A.F. Takács, M. Neumann, S. Simon, Local order changes induced in calcium–sodium–phosphate glasses by transition metals, Solid State Ionics 178 (2007) 221. https://doi.org/10.1016/j.ssi.2006.12.011

[31] B. Demri, D. Muster, XPS study of some calcium compounds, J. Mater. Process. Technol. 55 (1995) 311 https://doi.org/10.1016/0924-0136(95)02023-3

[32] W.E. Morgan, J.R. Van Wazer, W.J. Stec, Inner-orbital photoelectron spectroscopy of the alkali metal halides, perchlorates, phosphates, and pyrophosphates, J. Am. Chem. Soc. 95 (1973) 751 https://doi.org/10.1021/ja00784a018

[33] H.F. Franzen, J. Merrick, M. Umana, A.S. Khan, D.T. Peterson, J.R. McCreary, X-ray photoelectron studies of Ca, Sr and Ba and their oxides and carbonates, Thorn R.J., J. Electron Spectrosc. Relat. Phenom. 11 (1977) 439 https://doi.org/10.1016/0368-2048(92)85002-O

[34] D. Dixit, V. Soppina, C. Ghoroi, A Non-electric and Affordable Surface Engineered Particle (SEP) based Point-of-Use (POU) Water Disinfection System. Scientific Reports 9(1) (2019) 18245. DOI:10.1038/s41598-019-54602-3

[35] Christie, A.B., Lee J., Sutherland I., Walls J.M., An XPS study of ion-induced compositional changes with group II and group IV compounds, Appl. Surf. Sci. 15 (1983) 224, https://doi.org/10.1016/0378-5963(83)90018-1

[36] Y.M. Moustafa, K. El-Egili, Infrared spectra of sodium phosphate glasses, J. Non Cryst. Solids 240 (1–3) (1998) 144–153, https://doi.org/10.1016/S0022-3093(98)00711-X

[37] D. Carta, D.M. Pickup, J.C. Knowles, I. Ahmed, M.E. Smith, R.J. Newport, A structural study of sol-gel and melt-quenched phosphate-based glasses, J. Non Cryst. Solids 353 (18–21) (2007) 1759–1765, https://doi.org/10.1016/j.jnoncrysol.2007.02.008

[38] P.Y. Shih, Properties and FTIR spectra of lead phosphate glasses for nuclear waste immobilization, Mater. Chem. Phys. 80 (1) (2003) 299–304, https://doi.org/10.1016/S0254-0584(02)00516-3

[39] I. Konidakis, C.P.E. Varsamis, E.I. Kamitsos, D. Moncke, D. Ehrt, Structure and properties of mixed strontium-manganese metaphosphate glasses, J. Phys. Chem. C 114 (19) (2010) 9125–9138, https://doi.org/10.1021/jp101750t

[40] S. Lee, T. Nakano, T. Kasuga, Structure, dissolution behavior, cytocompatibility, and antibacterial activity of silver-containing calcium phosphate invert glasses, J. Biomed. Mater. Res. Part A 105 (11) (2017) 3127–3135, https://doi.org/10.1002/jbm.a.36173

[41] R. Scholz, R.L. Frost, Y.F. Xi, L.M. Graca, L. Lagoeiro, A. Lopez, Vibrational spectroscopic characterization of the phosphate mineral phosphophyllite - $Zn_2Fe(PO_4)(_2)$center dot $4H(_2)O$, from Hagendorf Sud, Germany and in comparison with other zinc phosphates, J. Mol. Struct. 1039 (2013) 22–27, https://doi.org/10.1016/j.molstruc.2013.01.075

[42] M. Dussauze, E. Kamitsos, F. Evelyne, V. Rodriguez, Structural rearrangements and second-order optical response in the space charge layer of thermally poled sodium-niobium

borophosphate glasses, J. Phys. Chem. C 111 (2007) 14560–14566, https://doi.org/10.1021/jp074335f

[43] C.Y. Kim, A.E. Clark, L.L. Hench, Early stages of calcium-phosphate layer formation in bioglasses, J. Non Cryst. Solids 113 (2–3) (1989) 195–202, https://doi.org/10.1016/0022-3093(89)90011-2

[44] Mneimne, M.; Hill, R.G.; Bushby, A.J.; Brauer, D.S. High phosphate content significantly increases apatite formation of fluoridecontaining bioactive glasses. Acta Biomater., 7 (2011) 1827–1834.

[45] G. Walter, J. Vogel, U. Hoppe, P. Hartmann, The structure of $CaO{-}Na_2O{-}MgO{-}P_2O_5$ invert glass. J. Non. Cryst. Solids 296 (2001) 212–223.

[46] A.R. Boccaccini, D.S. Brauer, L. Hupa, Bioactive Glasses: Fundamentals, Technology and Applications, Royal Society of Chemistry, 2016.

[47] S. Ali, Elastic properties and hardness of mixed alkaline earth silicate oxynitride glasses. Materials 14 (2022) 5022.

[48] S. Ali, A. Ellison, J. Luo, M. Edén, Composition–structure–property relationships of transparent Ca–Al–Si–O–N oxynitride glasses: The roles of nitrogen and aluminum. J. Am Ceram Soc. (2022) 1–18. https://doi.org/10.1111/jace.18866

[49] N.A. Wójcik, S. Ali, J.L. Karczewski, B. Jonson, M. Bartmański, R.J. Barczyński: D.C. and A.C. conductivity, biosolubility and thermal properties of Mg doped Na_2O-CaO-P_2O_5 glasses. Materials 14 (2021) 2626.